Dalton Transactions

Cite this: *Dalton Trans.*, 2012, **41**, 2066

www.rsc.org/dalton

PAPER

Ruthenium(II)/(III) complexes of 4-hydroxy-pyridine-2,6-dicarboxylic acid with PPh_3/$AsPh_3$ as co-ligand: Impact of oxidation state and co-ligands on anticancer activity *in vitro*†

Thangavel Sathiya Kamatchi,[a] Nataraj Chitrapriya,[b] Hyosun Lee,*[b] Chris F. Fronczek,[c] Frank R. Fronczek[c] and Karuppannan Natarajan*[a]

Received 5th July 2011, Accepted 31st October 2011
DOI: 10.1039/c1dt11273b

With the aim to develop more efficient, less toxic, target specific metal drugs and evaluate their anticancer properties in terms of oxidation state and co-ligand sphere, a sequence of Ru^{II}, Ru^{III} complexes bearing 4-hydroxy-pyridine-2,6-dicarboxylic acid and PPh_3/$AsPh_3$ were synthesized and structurally characterized. Biological studies such as DNA binding, antioxidant assays and cytotoxic activity were carried out and their anticancer activities were evaluated. Interactions of the complexes with calf thymus DNA revealed that the triphenylphosphine complexes could bind more strongly than the triphenylarsine complexes. The free radical scavenging ability, assessed by a series of *in vitro* antioxidant assays involving DPPH radical, hydroxyl radical, nitric oxide radical, superoxide anion radical, hydrogen peroxide and metal chelating assay, showed that the Ru^{III} complexes possess excellent radical scavenging properties compared to those of Ru^{II}. Cytotoxicity studies using three cancer lines *viz* HeLa, HepG2, HEp-2 and a normal cell line NIH 3T3 showed that Ru^{II} complexes exhibited substantial cytotoxic specificity towards cancer cells. Furthermore, the Ru^{II} complexes were found to be superior to Ru^{III} complexes in inhibiting the growth of cancer cells.

Introduction

Metal complexes offer infinite opportunities for the design of compounds with bioactivity due to the large variety of available metals and the ability to tune the reactivity and structure of the metal complexes by their ligand spheres.[1] In general, the nature of the metal ion, its oxidation state, the types and number of bound ligands and isomers of the complex can all exert a critical influence on the biological activity of a metal complex.[2–4] An understanding of how these factors affect biological activity should enable the design of metal complexes with specific medicinal properties. The wide spectrum of contrasting biological activity amongst platinum complexes[5–7] and the clinical success of Pt^{II} diam(m)ine complexes, *e.g.* cisplatin, as anticancer drugs provide a good illustration of this point.

Although 70% of all cancer patients receive cisplatin during cancer treatment, chemotherapy with cisplatin and its analogues still has several drawbacks; toxic side-effects and lack of activity (drug resistance) against several types of cancer are problems which need to be overcome.[8] This provides the impetus for the search for anticancer activity amongst complexes of other metals. At this juncture, ruthenium, a rare transition metal of the platinum group, has emerged as an attractive alternative due to several favorable properties suited to rational anticancer drug design and biological applications. Biologically compatible ligand-exchange kinetics of Ru^{II} and Ru^{III} similar to those of platinum complexes, a higher coordination number that could potentially be used to fine-tune the properties of the complexes, and lower toxicity (than their platinum counterparts) towards healthy tissues by mimicking iron in binding to many biological molecules are the advantages of using ruthenium complexes.[9,10]

The entrance of two Ru^{III} based drugs, NAMI-A[11] and KP1019[12] (Fig. 1) into clinical trials for the treatment of metastatic tumors

[a]*Department of Chemistry, Bharathiar University, Coimbatore, 641046, India. E-mail: k_natraj6@yahoo.com; Fax: +91-422-2422387; Tel: +91-422-2428319*
[b]*Department of Chemistry and Green-Nano Materials Research Center, Kyungpook National University, 1370 Sankyuk-dong, Buk-gu, Deagu, 702-701, Republic of Korea. E-mail: hyosunlee@knu.ac.kr; Fax: +82-53-950-6330; Tel: +82-53-950-5337*
[c]*Department of Chemistry, Louisiana State University, Baton Rouge, LA, 70803, USA*

† Electronic supplementary information (ESI) available: ^{1}H NMR spectrum of the complex [Ru^{II}-hpa-P] (Fig. S1). Cyclic voltammetric response of [Ru^{II}-hpa-P] (Fig. S2). X-Ray crystal structure and atom numbering scheme for [Ru^{III}-hpa-As] (Fig. S3). Hydrogen-bonding distances and angles (Table S1). Plot of $(\varepsilon_a-\varepsilon_f)/(\varepsilon_b-\varepsilon_f)$ *vs.* [DNA] for the titration of DNA with complexes. Emission spectra of EB bound to DNA in the absence and presence of [Ru^{III}-hpa-P]. Stern–Volmer quenching plot of EB bound to CT-DNA by ruthenium complexes (Fig. S4–S6). Antioxidant activity of all the complexes against various radicals (Fig. S7). Concentration effect curves of the complexes against HeLa, HepG2, HEp-2 and NIH 3T3 cell lines (Fig. S8–S11). CCDC reference numbers 797111–797113. For ESI and crystallographic data in CIF or other electronic format see DOI: 10.1039/c1dt11273b

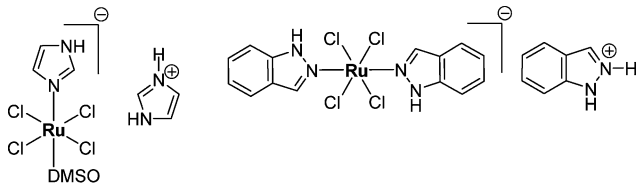

Fig. 1 Chemical structures of promising ruthenium drug candidates under investigation: NAMI-A and KP1019.

increased the interest in this metal. Both complexes behave quite differently from cisplatin *in vivo*. In addition, a number of Ru^{II} compounds were recently shown to possess very encouraging cytotoxic and antitumor properties in preclinical models[13,14] and are now under active investigation.

Bidentate carboxylate ligands have been used to endow cisplatin derivatives with high aquatic solubility and resistance to hydrolysis.[15] Two such examples, carboplatin and oxaliplatin, are used routinely in clinical practice. So, as a chelating partner to ruthenium, 4-hydroxy-pyridine-2,6-dicarboxylic acid (H_2hpa) is chosen due to its effective contribution in anti HIV investigation[16] and its valuable participation in anticancer activities.

Since the metal ion, its oxidation state and chelating ligand sphere play vital roles in determining chemical properties, and hence biological activities, a series of Ru^{II} and Ru^{III} complexes enclosing 4-hydroxy-pyridine-2,6-dicarboxylic acid were synthesized and structurally characterized. To obtain insight into the influence of the co-ligands, triphenylphosphines are replaced by triphenylarsines. All the complexes were subjected to biological studies such as DNA binding, antioxidant assays and cytotoxic activity testing.

Experimental section

Equipment and techniques

Melting points were determined with a Lab India instrument. Elemental analyses (C, H, N, S) were performed on a Vario EL III Elementar elemental analyzer. A Nicolet Avatar Model FT-IR spectrophotometer was used to record the IR spectra (4000–400 cm^{-1}) of the free ligand and the complexes. Fluorescence spectra were measured on a Perkin Elmer spectrofluorimeter. ^{1}H NMR spectra were recorded on Bruker AMX 500 at 500 MHz using tetramethylsilane as an internal standard. The electrochemical analyzer (CHI 1120A) equipped with a three electrode compartment consisting of platinum disc working electrode, platinum wire counter electrode and Ag/AgCl reference electrode was used to record the cyclic voltammograms of the complexes.

Materials

Commercially available $RuCl_3{\cdot}3H_2O$ (Himedia) was used without further purification. The starting complexes [RuHCl(CO)$(PPh_3)_3$],[50] [RuHCl(CO)$(AsPh_3)_3$],[51] [$RuCl_3(PPh_3)_3$],[52] [$RuCl_3(AsPh_3)_3$],[53] were prepared as reported earlier. 4-Hydroxy-pyridine-2,6-dicarboxylic acid was purchased from Acros organics and used as supplied. Solvents were purified and dried according to standard procedures.[54] Calf thymus DNA (CT-DNA) was purchased from Sigma and dissolved in 5 mM Tris HCl buffer (pH 7.0) containing 100 mM NaCl and 1 mM EDTA. It was dialyzed several times against 5 mM Tris HCl buffer. All experiments involving interactions of complexes with CT-DNA were carried out in Tris HCl buffer (pH 7.0). The concentrations of DNA, complexes [Ru^{II}(hpa)$(PPh_3)_2$CO], [Ru^{II}(hpa)$(AsPh_3)_2$CO], [Ru^{III}(hpa)$(PPh_3)_2$Cl] and [Ru^{III}(hpa)$(AsPh_3)_2$Cl] were determined spectrophotometrically using their extinction coefficients ε_{258nm} = 6700 M^{-1} cm^{-1}, ε_{330nm} = 9750 M^{-1} cm^{-1}, ε_{330nm} = 26 330 M^{-1} cm^{-1}, ε_{357nm} = 8345 M^{-1} cm^{-1} and ε_{330nm} = 27 620 M^{-1} cm^{-1} respectively.

Syntheses

Synthesis of complexes [Ru(hpa)$(EPh_3)_2$D] (E = P or As; D = CO or Cl). The new Ru^{II} and Ru^{III} complexes were synthesized by the following general procedure. An ethanolic (20 mL) solution of the H_2hpa (0.020 g, 0.099 mmol) was added to a refluxing solution of [RuHCl(CO)$(EPh_3)_3$], (0.095 g, 0.099 mmol; 0.108 g, 0.099 mmol) or [$RuCl_3(EPh_3)_3$] (0.098 g, 0.099 mmol; 0.112 g, 0.099 mmol) in ethanol (20 mL) (where E = P, As). The mixture was heated under reflux for 3 h. The solution was filtered while hot, reduced to half of its volume and left for slow evaporation. The semi crystalline product that separated out was filtered off, washed with ethanol and dried under vacuum.

Synthesis of [Ru(hpa)$(PPh_3)_2$(CO)] ([Ru^{II}-hpa-P]). The complex was synthesized from [RuHCl(CO)$(PPh_3)_3$] and H_2hpa. Orange crystals of the product were obtained by recrystallization from a chloroform/ethanol mixture. Yield = 0.076 g, 92%; m.p. >300 °C; elemental analysis calcd.(%) for $C_{44}H_{33}NO_6P_2Ru$: C, 63.31; H, 3.98; N, 1.68%. Found: C, 63.38; H, 3.99; N, 1.67%; UV-visible: λ_{max} (5%DMSO/H_2O)/nm 263 (ε/dm^3 mol^{-1} cm^{-1} 34 253) and 330 (9750); IR (KBr disks, ν_{max}/cm^{-1}) 3446 (OH); 1635 (COO, asymm); 1429 (COO, symm); 1917 (C≡O); ^{1}H NMR; δ_H (500MH_Z; [D_6] DMSO; 25 °C, TMS): 11.72 (1H, s, OH), 6.60 (2H, s, CH), 7.16–7.49 (30H, m, Ph), 1.06 (6H, t, J = 6.5 Hz, CH_3CH_2OH), 3.42–3.47 (4 H, m, CH_3CH_2OH), 4.35 (2H, t, J = 5 Hz, CH_3CH_2OH).

Synthesis of [Ru(hpa)$(AsPh_3)_2$(CO)] ([Ru^{II}-hpa-As]). The complex was synthesized from [RuHCl(CO)$(AsPh_3)_3$] and H_2hpa. Yield = 0.087g, 95%; m.p. >300 °C; elemental analysis calcd. (%) for $C_{44}H_{33}NO_6As_2Ru$: C, 57.28; H, 3.61; N, 1.52%. Found: C, 57.17; H, 3.60; N, 1.51%; λ_{max} (5%DMSO/H_2O)/nm 257 (ε/dm^3 mol^{-1} cm^{-1} 126 070) and 330 (26 330); IR (KBr disks, ν_{max}/cm^{-1}) 3410 (OH); 1620 (COO, asymm); 1443 (COO, symm); 1960 (C≡O); ^{1}H NMR δ_H (500MH_Z; [D_6] DMSO; 25 °C, TMS): 11.69 (1H, s, OH), 6.58 (2H, s, CH), 7.13–7.49 (30H, m, Ph).

Synthesis of [Ru(hpa)$(PPh_3)_2$(Cl)] ([Ru^{III}-hpa-P]). This was synthesized from [$RuCl_3(PPh_3)_3$] and H_2hpa. Red crystals of X-ray quality were grown by recrystallization from a dichloromethane/acetonitrile mixture. Yield = 0.070, 84%; m.p. >300 °C; elemental analysis calcd. (%) for $C_{43}H_{33}NO_5ClP_2Ru$: C, 61.32; H, 3.95; N, 1.66%. Found: C, 61.45; H, 3.93; N, 1.67%; λ_{max} (5%DMSO/H_2O)/nm 259 (ε/dm^3 mol^{-1} cm^{-1} 18 380), 327 (10 244) and 357 (8345); NIR (KBr disks, ν_{max}/cm^{-1}) 3433 (OH); 1650 (COO, asymm); 1442 (COO, symm).

Synthesis of [Ru(hpa)$(AsPh_3)_2$(Cl)] ([Ru^{III}-hpa-As]). This was prepared from [$RuCl_3(AsPh_3)_3$] and H_2hpa. Red crystals of

X-ray quality were obtained by recrystallization from a dichloromethane/acetonitrile mixture. Yield = 0.081g, 88%; m.p. >300 °C; elemental analysis calcd. (%) for $C_{43}H_{33}NO_5ClAs_2Ru$: C, 55.53; H, 3.58; N, 1.51%. Found: C, 55.42; H, 3.59; N, 1.52; λ_{max} (5%DMSO/H_2O)/nm 256 (ε/dm^3 mol^{-1} cm^{-1} 77 760) and 330 (27 620); IR (KBr disks, ν_{max}/cm^{-1}) 3419 (OH); 1638 (COO, asymm); 1432(COO, symm).

Crystallography: Data collection and structure determination

X-ray diffraction measurements were performed on a Nonius KappaCCD diffractometer equipped with an Oxford Cryostream chiller and graphite monochromated Mo-Kα radiation. The structures of all the three complexes were solved by direct methods and refinements were carried out by full matrix least-squares techniques. The hydrogen atoms were placed in idealized positions, except for those on OH, for which positions were refined. All three structures were solvates, [Ru^{II}-hpa-P] with ordered EtOH and disordered $CHCl_3$, [Ru^{III}-hpa-P] with disordered MeCN/DCM, and [Ru^{III}-hpa-As] with ordered MeCN. Contribution to the structure factors by disordered solvent in [Ru^{II}-hpa-P] was removed for refinement using the SQUEEZE[55] procedure, amounting to 0.64 molecules of disordered chloroform per Ru complex. Solvent in [Ru^{III}-hpa-P] was modeled as MeCN and DCM sharing a site in a 9 : 1 ratio. The following computer programs were used: structure solution SIR-97,[56] refinement SHELXL-97,[57] molecular diagrams, ORTEP-3[58] for Windows.

DNA binding experiments

The experiments were carried out in 5 mM Tris-HCl buffer (pH 7.0) at ambient temperature and the complexes were dissolved in 5 mM Tris-HCl buffer containing 5% DMSO. Changes in the fluorescence emission spectrum of the ethidium bromide (referred to as EB)-DNA complex were recorded under various complex concentrations. The fluorescence spectra were obtained at an excitation wavelength of 522 nm and an emission wavelength of 584 nm. Melting profiles were measured at 260 nm by a Cary 300 spectrophotometer. Readings were recorded for every 1 °C raise in temperature per minute. The viscosity measurement was carried out using an Ubbelodhe viscometer immersed in a thermostatic water bath maintained at 25(±0.l) °C. DNA samples approximately 200 base pairs in length were prepared by sonication in order to minimize complexities arising from DNA flexibility. Flow times were measured with a digital stopwatch; each sample was measured three times, and an average flow time was calculated. Relative viscosities for CT-DNA in the presence and absence of the complex were calculated from the relation $\eta = (t - t_0)/t_0$, where t is the observed flow time of DNA-containing solution and t_0 is the flow time of Tris-HCl buffer alone. Data are presented as $(\eta/\eta_0)^{1/3}$ *versus* binding ratio, where η is the viscosity of CT-DNA in the presence of complex and η_0 is the viscosity of CT-DNA alone.

Antioxidant assays

The ability of ruthenium complexes to act as hydrogen donors or free radical scavengers was explored by conducting a series of *in vitro* antioxidant assays involving DPPH radical, hydroxyl radical, nitric oxide radical, hydrogen peroxide, superoxide anion radical, metal chelating assay and comparing the results with standard antioxidants, including the natural antioxidant vitamin C and the synthetic antioxidant BHT.

DPPH$^{\cdot}$ scavenging assay

The DPPH radical scavenging activity of the compounds was measured according to the method of Blios.[59] The DPPH radical is a stable free radical. Because of the odd electron, DPPH shows a strong absorption band at 517 nm in the visible spectrum. As this electron becomes paired off in the presence of a free radical scavenger, the absorption vanishes and the resulting decolorization is stoichiometric with respect to the number of electrons taken up. Various concentrations of the experimental complexes were taken and the volume was adjusted to 100 µL with methanol. About 5 mL of a 0.1 mM methanolic solution of DPPH was added to the aliquots of samples and standards (BHT and vitamin C) and shaken vigorously. A negative control was prepared by adding 100 µL of methanol in 5 mL of 0.1 mM methanolic solution DPPH. The tubes were allowed to stand for 20 min at 27 °C. The absorbance of the sample was measured at 517 nm against the blank (methanol).

OH$^{\cdot}$ scavenging assay

The hydroxyl radical scavenging activity of the complex has been investigated by using the Nash method.[60] *In vitro* hydroxyl radicals were generated by an Fe^{3+}/ascorbic acid system. The detection of hydroxyl radicals was carried out by measuring the amount of formaldehyde formed from the oxidation reaction with DMSO. The formaldehyde produced was detected spectrophotometrically at 412 nm. A mixture of 1.0 mL of iron-EDTA solution (0.13% ferrous ammonium sulphate and 0.26% EDTA), 0.5 mL of EDTA solution (0.018%), and 1.0 mL of DMSO (0.85% DMSO (v/v) in 0.1 M phosphate buffer, pH 7.4) were sequentially added in the test tubes. The reaction was initiated by adding 0.5 mL of ascorbic acid (0.22%) and was incubated at 80–90 °C for 15 min in a water bath. After incubation, the reaction was terminated by the addition of 1.0 mL of ice-cold trichloroacetic acid (17.5% w/v). Subsequently, 3.0 mL of Nash reagent was added to each tube and left at room temperature for 15 min. The intensity of the colour formed was measured spectrophotometrically at 412 nm against reagent blank.

NO$^{\cdot}$ scavenging assay

The assay of nitric oxide (NO$^{\cdot}$) scavenging activity is based on a method[61] in which sodium nitroprusside in aqueous solution at physiological pH spontaneously generates nitric oxide, which interacts with oxygen to produce nitrite ions. These can be estimated using the Greiss reagent. Scavengers of nitric oxide compete with oxygen leading to reduced production of nitrite ions. For the experiment, sodium nitroprusside (10 mM) in phosphate buffered saline was mixed with a fixed concentration of the complex and standards and incubated at room temperature for 150 min. After the incubation period, 0.5 mL of Griess reagent containing 1% sulfanilamide, 2% H_3PO_4 and 0.1% *N*-(1-naphthyl) ethylenediamine dihydrochloride was added. The absorbance of the chromophore formed was measured at 546 nm.

H_2O_2 scavenging assay

The ability of the complexes to scavenge hydrogen peroxide was determined using the method of Ruch *et al.*[62] A solution of hydrogen peroxide (2.0 mM) was prepared in phosphate buffer (0.2 M, pH 7.4) and its concentration was determined spectrophotometrically from absorption at 230 nm with molar absorptivity 81 M^{-1} cm^{-1}. The complexes (100 μg mL^{-1}), BHT and vitamin C (100 μg mL^{-1}) were added to 3.4 mL of phosphate buffer together with hydrogen peroxide solution (0.6 mL). An identical reaction mixture without the sample was taken as negative control. Absorbance of hydrogen peroxide at 230 nm was determined after 10 min against the blank (phosphate buffer).

$O_2^{-\bullet}$ scavenging assay

The superoxide anion radical ($O_2^{-\bullet}$) scavenging assay was based on the capacity of the complexes to inhibit formazan formation by scavenging the superoxide radicals generated in the riboflavin-light-NBT system.[63] Each 3 mL reaction mixture contained 50 mM sodium phosphate buffer (pH 7.6), 20 μg riboflavin, 12 mM EDTA, 0.1 mg NBT and 1 mL complex solution (20–100 μg mL^{-1}). The reaction was started by illuminating the reaction mixture with different concentrations of complex for 90 s. Immediately after illumination, the absorbance was measured at 590 nm. The entire reaction assembly was enclosed in a box lined with aluminum foil. Identical tubes with the reaction mixture kept in the dark served as blanks.

Metal chelating activity

The chelation with ferrous ions by the experimental complexes was estimated by the method of Dinis *et al.*[64] Initially, about 100 μL the samples and the standards were added to 50 μL solution of 2 mM $FeCl_2$. The reaction was initiated by the addition of 200 μL of 5 mM ferrozine and the mixture was shaken vigorously and left standing at room temperature for 10 min. Absorbance of the solution was then measured spectrophotometrically at 562 nm against the blank (deionized water).

For the above six assays, all the tests were run in triplicate and the percentage activity was calculated by the following equation

$$\text{Scavenging activity (\%)} = [(A_0 - A_1) / A_0] \times 100$$

where A_0 is the absorbance of the control and A_1 is the absorbance of the complex/standard. When the percentage inhibition of the tested compounds is 50%, the tested compound concentration is the IC_{50} value.

In vitro anticancer activity evaluation by MTT assay

Cytotoxicity studies of the complexes and cisplatin were carried out on human cervical cancer cells (HeLa), human laryngeal epithelial carcinoma cells (HEp-2), human liver carcinoma cells (HepG2) and mouse embryonic fibroblasts (NIH 3T3), all of which were obtained from National Centre for Cell Science (NCCS), Pune, India. Cell viability was carried out using the MTT assay method.[65] The HeLa, HepG2 and HEp-2 cells were grown in Eagles minimum essential medium containing 10% fetal bovine serum (FBS) and NIH 3T3 fibroblasts were grown in Dulbeccos modified Eagles medium (DMEM) containing 10% FBS. For screening experiments, the cells were seeded into 96-well plates in 100 μL of the respective medium containing 10% FBS, at a plating density of 10 000 cells/well and incubated at 37 °C, 5% CO_2, 95% air and 100% relative humidity for 24 h prior to the addition of compounds. The compounds were dissolved in DMSO and diluted in the respective medium containing 1% FBS. After 24 h, the medium was replaced with the respective medium with 1% FBS containing the compounds at various concentrations and incubated at 37 °C, 5% CO_2, 95% air and 100% relative humidity for 48 h. Experiments were performed in triplicate and the medium without the compounds served as control. After 48 h, 10 μL of MTT (5 mg mL^{-1}) in phosphate buffered saline (PBS) was added to each well and incubated at 37 °C for 4 h. The medium with MTT was then removed and the formed formazan crystals were dissolved in 100 μL of DMSO and the absorbance measured at 570 nm using a micro plate reader. The % cell inhibition was determined using the following formula, and a graph was plotted between % of cell inhibition and concentration. From this plot, the IC_{50} value was calculated.

$$\%\ \text{inhibition} = [\text{mean OD of untreated cells (control)} / \text{mean OD of treated cells (control)}] \times 100.$$

Results and discussion

Reactions of H_2hpa with $[RuCl_3(EPh_3)_3]$ and $[RuHCl(CO)(EPh_3)_3]$ gave new complexes of the type $[Ru(hpa)(EPh_3)_2D]$ as shown in Scheme 1. The analytical data confirmed the molecular formulae for the new complexes. It has been observed that one molecule of the dicarboxylic acid replaced a chloride ion, a hydride ion and a $PPh_3/AsPh_3$ in the case of Ru^{II} complexes, two chlorides and a $PPh_3/AsPh_3$ in the case of Ru^{III} complexes. X-ray crystal determinations revealed that the dicarboxylic acid coordinated to the metal ion as dibasic tridentate ONO donor.

Electrochemistry

Redox behaviors of the ligand and new Ru^{II} and Ru^{III} complexes have been evaluated by means of cyclic voltammetry using their methylene chloride solutions containing 0.1 M tetrabutylammonium perchlorate (~1×10^{-3} M) as a supporting electrolyte. The solution was degassed with a continuous flow of nitrogen before scanning. All the complexes are electroactive with respect to the ligand and metal centre. The complexes show different redox behaviors in the chosen potential window of ±2 V at a scan rate of 50 mV s^{-1}. The complexes display two successive one electron reductions and an oxidation. The redox process is best described as reversible/quasireversible electron transfer borne out by the fact that the peak-to-peak separation value ($E_{pa} - E_{pc}$) ranges from 83–240 mV. There is little variation in the cyclic voltammograms when triphenylphosphine is replaced by triphenylarsine in the complexes. Hence, the redox behavior of the complexes **[Ru^{II}-hpa-P]** and **[Ru^{III}-hpa-P]** will be described in detail here. The electrochemical data are given in Table 1. A representative voltammogram is given in Fig. S2, ESI.†

Electrochemical behavior of [Ru^{II}-hpa-P]. **[Ru^{II}-hpa-P]** exhibited a reversible reduction couple with $E_{1/2}$ value −1.15 V and peak-to-peak separation of 83 mV which can be assigned to the one electron Ru^{II}/Ru^{I} redox process. The calculated $E_{1/2}$

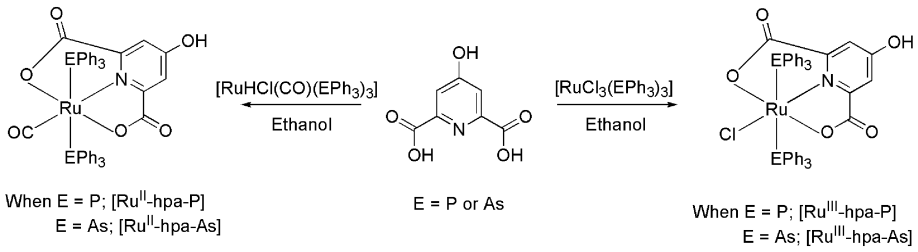

Scheme 1 General scheme for the synthesis of new ruthenium complexes.

Table 1 Cyclic voltammetric data of the complexes and their estimated redox potentials

Complex	Reduction[c]	E_f[a] (V)/ΔE_p[b] (mV) ligand based reduction[d]	Oxidation[e]
[Ru^{II}-hpa-P]	−1.15/083	−0.58/225	1.45/161
[Ru^{II}-hpa-As]	−1.17/117	−0.60/220	1.45/142
[Ru^{III}-hpa-P]	−1.17/210	−0.47/176	1.46/147
[Ru^{III}-hpa-As]	−1.17/240	−0.48/225	1.47/195
Free Ligand (H_2hpa)		−0.52/147	

[a] E_f = formal potential calculated as the average of anodic (E_{pa}) and cathodic (E_{pc}) peak potentials. [b] ΔE_p = Peak-to-Peak separation ($E_{pa}-E_{pc}$). [c] Ru^{I}/Ru^{II} and Ru^{II}/Ru^{III}. [d] hpa/hpa$^{\bullet-}$ and H_2hpa/H_2hpa$^{\bullet-}$. [e] Ru^{III}/Ru^{II} and Ru^{IV}/Ru^{III}.

values are concurrent with the literature reports.[17,18] In addition, a quasi-reversible cathodic process occurring at –0.58 V *versus* Ag/Ag^+ with peak-to-peak separation of 225 mV can be safely assigned to a ligand based redox response on comparing with the electrochemical data of H_2hpa and it is attributed to the formation of the hpa radical anion. An oxidation couple observed with formal potential 1.45 V is quasi-reversible (ΔE_p = 161 mV) and it is assigned to the Ru^{III}/Ru^{II} redox process. From this, it is inferred that the Ru^{II} complex favors the reduction process to Ru^{I} rather than the oxidation process to Ru^{III}.

Electrochemical behavior of [Ru^{III}-hpa-P]. **[Ru^{III}-hpa-P]** displayed a well-defined one-electron quasi-reversible coupled redox wave on either side of the reference electrode besides a quasi-reversible redox response at less negative potentials with respect to the coupled redox wave at the negative side of the Ag/AgCl electrode. The complex gave a quasi-reversible cyclic voltammetric response due to the Ru^{III}–Ru^{II} couple at $E_{1/2}$ = –1.17 V with peak-to-peak separation (ΔE_p) of 210 mV. This is attributed to slow electron transfer and adsorption of the complexes onto the electrode surface.[19] A quasi-reversible ligand based reduction at –0.47 V with ΔE_p = 176 mV was also observed. In addition, metal centered oxidation occurred at 1.46 V with ΔE_p = 147 mV ascribed to a quasi-reversible one electron Ru^{IV}/Ru^{III} redox process.

X-ray crystallography

General. The structures of **[Ru^{II}-hpa-P], [Ru^{III}-hpa-P]** and **[Ru^{III}-hpa-As]** have been established by single crystal X-ray analysis. The ORTEP style drawings of **[Ru^{II}-hpa-P]** and **[Ru^{III}-hpa-P]** are displayed in Fig. 2 and 3. The details concerning the data collection and structure refinement of the complexes are summarized in Table 2. The ORTEP diagram of **[Ru^{III}-hpa-As]** (Fig. S3, ESI†), selected geometrical parameters (interatomic distances and angles) and

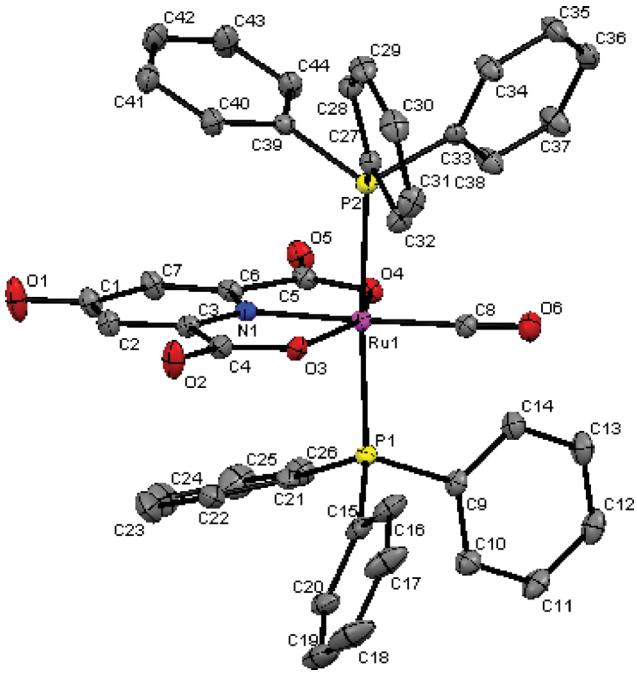

Fig. 2 X-ray crystal structure and atom numbering scheme for **[Ru^{II}-hpa-P]** as thermal ellipsoids at a 50% probability level. The hydrogen atoms have been omitted for clarity.

hydrogen bond distances are given in Table 3 and Table S1, ESI† respectively.

Crystal structure of [Ru^{II}-hpa-P]

Single crystals of **[Ru^{II}-hpa-P]** were obtained from slow evaporation of a mixture of chloroform and ethanol at room temperature. An orange single crystal of approximate unit cell dimensions 0.25 × 0.20 × 0.17 mm was isolated and the single crystal X-ray diffraction experiments were carried out at 90 K. From the unit cell dimensions, it is clear that the crystal is triclinic belonging to the $P\bar{1}$ space group. The crystal was a solvate containing ethanol and disordered chloroform.

The Ru^{II} ion exhibits hexa coordination with an octahedral geometry where equatorial coordination comes from two carboxylate oxygen atoms, the ring nitrogen of the tridentate chelating ligand H_2hpa and a carbonyl carbon. A pair of triphenylphosphine ligands completes the axial coordination. The coordination environment around the Ru^{II} ion can be considered as being a distorted octahedron {$RuNO_2P_2(CO)$} because of distortions of the bond angles (Table S3, ESI†) from the required 90°and 180° at the basal plane which is reflected in the bonding parameters

Table 2 Crystallographic data for **[Ru^{II}-hpa-P]**, **[Ru^{III}-hpa-P]** and **[Ru^{III}-hpa-As]**

	[Ru^{II}-hpa-P]	**[Ru^{III}-hpa-P]**	**[Ru^{III}-hpa-As]**
CCDC deposit number	797111	797112	797113
Empirical formula	$C_{44}H_{33}NO_6P_2Ru\cdot2(C_2H_6O)\cdot0.64(CHCl_3)$	$C_{43}H_{33}ClNO_5P_2Ru\cdot0.9(C_2H_3N)\cdot0.1(CH_2Cl_2)$	$C_{43}H_{33}As_2ClNO_5Ru\cdot C_2H_3N$
Formula weight	1003.26	887.61	971.1
T (K)	90	90	90
Wavelength (Å)	0.71073	0.71073	0.71073
Crystal system	Triclinic	Triclinic	Triclinic
Space group	$P\bar{1}$	$P\bar{1}$	$P\bar{1}$
Unit cell dimensions			
a (Å)	12.0057(14)	12.0311(15)	12.3411(14)
b (Å)	14.0262(15)	13.5729(15)	13.6920(15)
c (Å)	15.237(2)	13.996(2)	14.2068(15)
α (°)	89.650(5)	84.593(7)	82.983(6)
β (°)	81.378(5)	71.947(6)	69.879(5)
γ (°)	71.638(6)	64.431(7)	63.268(5)
Volume (Å^3)	2405.4(5)	1958.0(5)	2011.6(4)
Z	2	2	2
Density (calculated) Mg m^{-3}	1.385	1.505	1.603
Absorption coefficient mm^{-1}	0.551	0.614	2.138
F(000)	1030	906	974
Theta range for data collection	2.7 to 34.3°	1.5 to 32°	2.8 to 34.9°
Index ranges	−18 <= h <= 18, −21 <= k <= 21, −23 <= l <= 23	−17 <= h <= 17, −18 <= k <= 20, −20 <= l <= 20	−19 <= h <= 19, −21 <= k <= 21, −22 <= l <= 22
Reflections collected/unique, R_{int}	69 185/18 649, 0.042	53 880/13 603, 0.039	57 165/16 343, 0.042
Completeness to theta$_{max}$	0.931	0.997	0.932
Refinement method	Full-matrix least-squares on F^2	Full-matrix least-squares on F^2	Full-matrix least-squares on F^2
Data/restraints/parameters	18 649/0/545	13 603/0/530	16 343/0/508
Goodness-of-fit on F^2	1.091	1.065	1.032
Final R indices [$I > 2\sigma(I)$]	$R_1 = 0.044$, w$R_2 = 0.107$	$R_1 = 0.040$, w$R_2 = 0.102$	$R_1 = 0.039$, w$R_2 = 0.080$
R indices (all data)	$R_1 = 0.066$, w$R_2 = 0.114$	$R_1 = 0.065$, w$R_2 = 0.129$	$R_1 = 0.070$, w$R_2 = 0.089$
Largest diff. peak and hole	0.92 and −1.14 e. Å^{-3}	0.86 and −1.77e. Å^{-3}	1.14 and −1.08 e. Å^{-3}

Table 3 Selected geometrical parameters for **[Ru^{II}-hpa-P]**, **[Ru^{III}-hpa-P]** and **[Ru^{III}-hpa-As]**

Interatomic distances (Å)					
[Ru^{II}-hpa-P]		**[Ru^{III}-hpa-P]**		**[Ru^{III}-hpa-As]**	
Ru1–C8	1.867(2)	Ru1–Cl1	2.3402(6)	Ru1–Cl1	2.3381(6)
Ru(1)–O(3)	2.117(1)	Ru(1)–O(3)	2.046(2)	Ru(1)–O(3)	2.048(1)
Ru(1)–O(4)	2.123(1)	Ru(1)–O(4)	2.080(1)	Ru(1)–O(4)	2.075(1)
Ru(1)–N(1)	2.034(1)	Ru(1)–N(1)	2.015(2)	Ru(1)–N(1)	2.009(2)
Ru(1)–P(1)	2.3825(6)	Ru(1)–P(1)	2.399(6)	Ru(1)–As(1)	2.4691(4)
Ru(1)–P(2)	2.3704(6)	Ru(1)–P(2)	2.3848(7)	Ru(1)–As (2)	2.4637(4)
Bond angles (°)					
C(8)–Ru(1)–N(1)	177.24(7)	Cl(1)–Ru(1)–N(1)	175.63(6)	Cl(1)–Ru(1)–N(1)	175.47(5)
C(8)–Ru(1)–O(3)	101.39(7)	Cl(1)–Ru(1)–O(3)	98.44(5)	Cl(1)–Ru(1)–O(3)	98.19(5)
C(8)–Ru(1)–O(4)	104.97(7)	Cl(1)–Ru(1)–O(4)	107.79(5)	Cl(1)–Ru(1)–O(4)	107.69(4)
C(8)–Ru(1)–P(1)	91.23(6)	Cl(1)–Ru(1)–P(1)	88.95(2)	Cl(1)–Ru(1)–As(1)	88.88(2)
C(8)–Ru(1)–P(2)	85.86(6)	Cl(1)–Ru(1)– P(2)	86.47(2)	Cl(1)–Ru(1)–As(2)	86.66(2)
O(3)–Ru(1)–P(1)	93.22(4)	O(3)–Ru(1)–P(1)	94.23(5)	O(3)–Ru(1)–As(1)	94.45(4)
O(3)–Ru(1)–P(2)	91.57(4)	O(3)–Ru(1)–P(2)	90.53(5)	O(3)–Ru(1)–As(2)	90.59(4)
O(3)–Ru(1)–O(4)	153.64(5)	O(3)–Ru(1)–O(4)	153.75(7)	O(3)–Ru(1)–O(4)	154.10(6)
O(4)–Ru(1)–P(1)	85.94(4)	O(4)–Ru(1)–P(1)	85.55(5)	O(4)–Ru(1)–As(1)	85.24(4)
O(4)–Ru(1)–P(2)	90.66(4)	O(4)–Ru(1)–P(2)	91.91(5)	O(4)–Ru(1)–As(2)	91.88(4)
N(1)–Ru(1)–O(3)	76.86(5)	N(1)–Ru(1)–O(3)	77.20(7)	N(1)–Ru(1)–O(3)	77.32(7)
N(1)–Ru(1)–O(4)	76.82(5)	N(1)–Ru(1)–O(4)	76.57(7)	N(1)–Ru(1)–O(4)	76.80(7)
N(1)–Ru(1)–P(1)	90.99(4)	N(1)–Ru(1)–P(1)	91.79(6)	N(1)–Ru(1)–As(1)	92.10(5)
N(1)–Ru(1)–P(2)	92.04(4)	N(1)–Ru(1)–P(2)	93.09(6)	N(1)–Ru(1)–As(2)	92.68(5)
P(1)–Ru(1)–P(2)	174.81(2)	P(1)–Ru(1)–P(2)	173.83(2)	As(1)–Ru(1)–As(2)	173.71(1)

around the ruthenium atom. Though the PPh_3 ligands usually prefer to occupy mutually *cis* positions for better π-interaction,[20] in this complex the presence of CO, a stronger π-acidic ligand, might have forced the bulky PPh_3 ligands to take up mutually *trans* positions for steric reasons. The carbonyl group occupies the site *trans* to the N1 (ring nitrogen from H_2hpa (N1–Ru1–C8, 177.24(7) Å)). This may be a consequence of strong Ru^{II}→CO back donation as indicated by the short Ru–C bond (1.867(2) Å) and low CO stretching frequency (1917 cm^{-1}), which prefers σ or weak π donor groups occupying the site opposite to CO to favor the d–π* back donation. The Ru–C bond length of 1.867(2) Å in the Ru(CO) fragment is quite normal, similar to

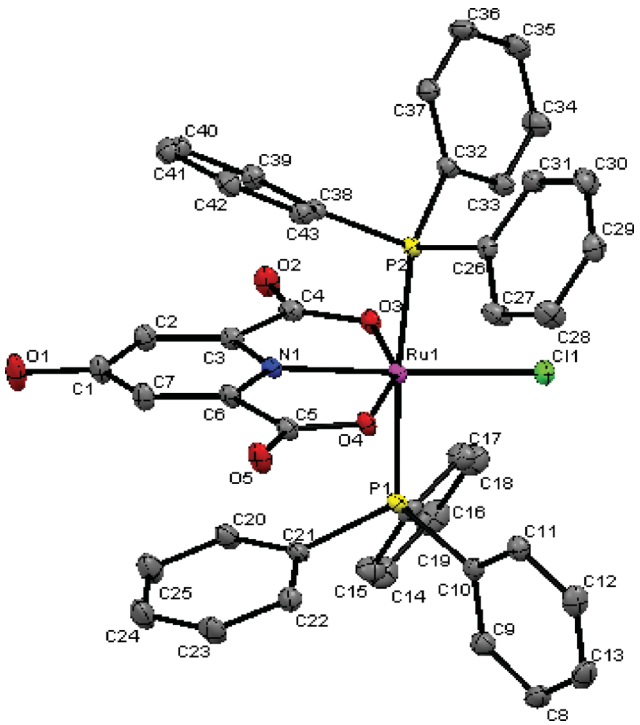

Fig. 3 X-ray crystal structure and atom numbering scheme for **[Ru^{III}-hpa-P]** as thermal ellipsoids at a 50% probability level. The hydrogen atoms have been omitted for clarity.

that observed in structurally characterized carbonyl complexes of ruthenium.[21–23] The two Ru–P bond lengths are similar and are comparable to those reported for other PPh_3 coordinated Ru^{II} complexes.[24,25]

The molecule is stabilized by intermolecular hydrogen bonding networks with lattice ethanol molecules and oxygen atoms of H_2hpa. Two ethanol molecules are solvated with the complex. One ethanol molecule is hydrogen bonded with an uncoordinated carboxylate oxygen atom O5 (H–Acceptor) of the H_2hpa. The hydroxyl group O1 (H–Donor), the carboxylate group O2 (H–Acceptor) of the neighboring molecule form hydrogen bonds to the other ethanol molecule. The oxygen atom of the other ethanol molecule acts as a donor to the uncoordinated carboxylate oxygen atom O2 of the neighboring molecule and as an acceptor to oxygen atom O1 of the hydroxyl group at the C1 atom of H_2hpa.

Structure of [Ru^{III}-hpa-P] and [Ru^{III}-hpa-As]

The coordination geometry around the Ru^{III} ion is a slightly distorted octahedron, where the basal plane is constructed of two oxygen atoms, the nitrogen of the tridendate dibasic ligand H_2hpa, and a chlorine atom. The remaining apical coordination sites are filled up by two triphenylphosphines/triphenylarsines. The coordination sphere is the same in the two Ru^{III} complexes and the general structural motifs are very similar with only very slight differences in the geometrical parameters. Thus, the structure of one of the Ru^{III} complexes, **[Ru^{III}-hpa-P]**, will be described in detail here.

The H_2hpa ligand coordinated equatorially to the metal with bite angles of 76.57(7)° and 77.20(7)°. This results in significant distortion of the $RuNO_2P_2Cl$ core from the ideal octahedral geometry, which is reflected in the twelve *cis* and three *trans* angles. The equatorial Ru–N [2.015(2) Å] Ru–O [2.046(2), 2.080(1)] Ru–Cl [2.0432(6) Å] and axial Ru–P [2.3990(8), 2.3848(7)] bond lengths indicate an axially elongated octahedral coordination environment around the Ru^{III} ion. The two triphenylphosphine ligands which are mutually *trans* to each other are slightly bent towards the chlorine atom due to the steric requirements of the somewhat bulky chelating ligand, H_2hpa causing a slight deviation from a linear *trans* arrangement, which is evident from the P(1)–Ru(1)–Cl(1) bond angle of 88.95(2)° [smaller than P(1)–Ru(1)–N(1) = 91.79(6)° and P(2)–Ru(1)–N(1) = 93.09(6)°]. The N(1)–Ru(1)–Cl(1) bond angle is 175.63(6)° showing that the Cl atom lies *trans* to the ring nitrogen. The Ru–P, Ru–O, Ru–N and Ru–Cl bond lengths found in the complex agree well with those reported for similar ruthenium complexes.[26–29] An acetonitrile and a dichloromethane molecule share a disordered site. Though the hydroxyl group at the C1 atom of H_2hpa does not take part in metal coordination, it is involved in intermolecular hydrogen bonding interactions with a neighboring carboxylate carbonyl O5 (H–Acceptor) atom. In addition, the complex possesses intermolecular interactions between nitrogen (from a solvated acetonitrile molecule) and chlorine (from a solvated dichloromethane molecule) and between chlorine and oxygen.

DNA binding studies

Electronic absorption titration. In order to elucidate the nature of the interaction of the complexes with DNA, UV-vis absorption spectra were obtained by titration of the complexes with increasing concentrations of DNA (Fig. 4). The titration processes were repeated until there was no change in the spectra indicating that binding saturation had been achieved. The electronic spectra of all the complexes showed an intense absorption peak around 259 nm in the UV region, which could be attributed to an intraligand π–π* transition of the coordinated groups in the complex and a lower energy absorption band around 330 nm. In addition to the above two bands, the complex **[Ru^{III}-hpa-P]** showed an additional MLCT band at 357 nm. The absorbance spectra of **[Ru^{III}-hpa-P]** and **[Ru^{II}-hpa-P]** were considerably affected upon binding to calf thymus DNA, as shown in Fig. 4 and subsequent changes are given in Table 4.

Clear isosbestic points at 300 nm for **[Ru^{III}-hpa-P]** and at 290 nm for **[Ru^{II}-hpa-P]** do reveal the presence of two spectroscopically distinct chromophores (free and bound) in the solution which indicate the occurrence of a single binding mode of the complexes with DNA. It was anticipated that the binding of **[Ru^{III}-hpa-P]** and **[Ru^{II}-hpa-P]** with DNA could be either by intercalation or by sitting within either the minor or major grooves of the DNA structure. As the *R* ratio increases, no isosbestic point was observed (data not shown). This is perhaps indicative of a heterogeneous

Table 4 Changes observed in λ for interaction of the complexes with CT-DNA

Complex	λ (nm)	Hypochromism	Red shift (nm)
[Ru^{III}-hpa-P]	330	39%	11
	357	36%	9
[Ru^{II}-hpa-P]	330	30%	—

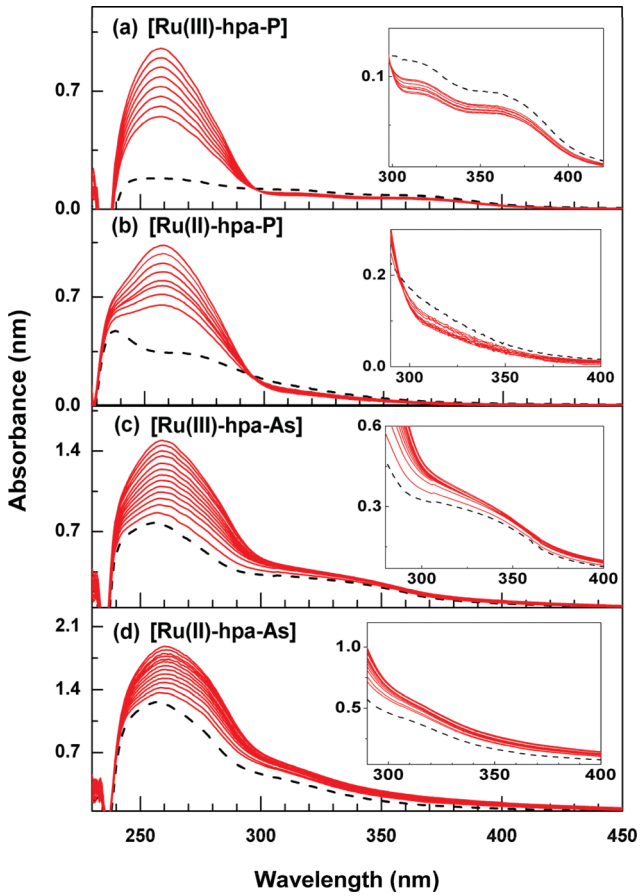

Fig. 4 UV spectra of ruthenium complexes in the absence (- - -) and in the presence of CT-DNA in increasing amounts, [Complex] = 10 μM, [DNA] = 0–130 μM.

binding of complexes for **[Ru^{III}-hpa-P]** and **[Ru^{II}-hpa-P]** at higher mixing ratios ($R > 0.16$).

In contrast, at various DNA concentrations, the absorption spectra of **[Ru^{II}-hpa-As]** and **[Ru^{III}-hpa-As]** exhibited hyperchromicity without a clear isosbestic point. These compounds may assume a different DNA binding mode from that of the other two. In other words, strong interaction may be ruled out as a major binding mode of **[Ru^{II}-hpa-As]** and **[Ru^{III}-hpa-As]** with the double helical DNA. The lack of an isosbestic point may suggest that its chromophore environment was not altered after the interaction with DNA. The observed hyperchromic effect for **[Ru^{II}-hpa-As]** and **[Ru^{III}-hpa-As]** suggested the binding could be *via* external contact (electrostatic binding).

Based on the above observations, we presume that there are some interactions between complexes **[Ru^{III}-hpa-P]**, **[Ru^{II}-hpa-P]** and DNA. The binding strength of the complex with DNA was further mirrored in the value of the intrinsic binding constant (K_b). The **[Ru^{III}-hpa-P]** and **[Ru^{II}-hpa-P]** exhibited a regular decrease in intensity of the absorption band from which the value of the intrinsic equilibrium binding constant (K_b) was calculated using

$$[DNA] / (\varepsilon_a - \varepsilon_f) = [DNA] / (\varepsilon_b - \varepsilon_f) + 1/K_b\ (\varepsilon_b - \varepsilon_f)$$

where [DNA] is the concentration of the DNA in base pairs, $\varepsilon_a = A_{obsd}$/[compound], ε_f is the extinction coefficient for the free compound and ε_b is the extinction coefficient for the compound in the fully DNA-bound form. Each set of data, when fitted to the above equation, gave a straight line with a slope of $1/(\varepsilon_b - \varepsilon_f)$ and a y-intercept of $1/K_b\ (\varepsilon_b - \varepsilon_f)$ and K_b was determined from the ratio of the slope to intercept.

The intrinsic binding constants K_b of **[Ru^{III}-hpa-P]** and **[Ru^{II}-hpa-P]** were found to be 1.3×10^4 and 4.6×10^3 M^{-1} respectively. Fig. S4, ESI† indicates that **[Ru^{III}-hpa-P]** binds more strongly than **[Ru^{II}-hpa-P]** to the double helix. The observed K_b values for **[Ru^{III}-hpa-P]** and **[Ru^{II}-hpa-P]** are lower than that of the classical intercalators (ethidium bromide, K_b, 1.8×10^6 M^{-1} in 25 mM Tris-HCl/40 mM NaCl buffer, pH 7.9) and partial intercalating metal complexes ($[Ru(phen)_2(dppz)]^{2+}$, $K_b > 10^6$ M^{-1}) bound to CT-DNA.[30] Hence, it is inferred that the interaction of the two complexes with DNA is nonintercalative.

Competitive studies with ethidium bromide

The new complexes show no fluorescence at room temperature in solution or in the presence of DNA, and their binding to DNA cannot be directly predicted through the emission spectra. The extent of quenching of the fluorescence of ethidium bromide (EB) bound to DNA is used to determine the binding of a second molecule to DNA.[31] This fluorescence based competition technique can provide indirect evidence for the DNA binding mode.[32] Fig. S5, ESI† shows the emission spectra of the EB-DNA system in the absence and presence of the complexes **[Ru^{III}-hpa-P]** and **[Ru^{II}-hpa-P]**. The fluorescence intensity of EB shows a remarkable decrease with increasing concentration of the complexes **[Ru^{III}-hpa-P]** and **[Ru^{II}-hpa-P]**, which is a consequence of the displacement of some EB molecules from the DNA. The addition of **[Ru^{III}-hpa-P]** to DNA pretreated with EB caused an appreciable reduction in emission intensity compared with that observed in the complex **[Ru^{II}-hpa-P]** at a lower mixing ratio ($R < 0.16$). This indicated that the complex **[Ru^{III}-hpa-P]** could strongly compete with EB in binding to DNA. As the R ratio ($R > 0.16$) increases, there is no appreciable change in the emission intensity of the EB-DNA system (data not shown). The complexes **[Ru^{II}-hpa-As]** and **[Ru^{III}-hpa-As]** do not provoke any significant changes in the intensity of the emission band at 592 nm of the DNA-EB system indicating that they cannot displace EB from the DNA-EB complex. This trend indicates that there is only weak binding of complexes **[Ru^{II}-hpa-As]** and **[Ru^{III}-hpa-As]** with the CT-DNA. The binding constant K_b of complexes **[Ru^{II}-hpa-P]** and **[Ru^{II}-hpa-P]** to DNA can be analyzed through the Stern–Volmer equation

$$I_0 / I = 1 + K_{sq} r$$

where I_0 and I represent the fluorescence intensities in the absence and presence of the complex, respectively, and r is the concentration ratio of the complex to DNA. K_{sq} is a linear Stern–Volmer quenching constant dependent on the ratio of the bound concentration of EB to the concentration of DNA (Fig. S6, ESI†). In particular, the high K_{sq} values of the complexes show that they can be bound tightly to the DNA. The K_b values for **[Ru^{III}-hpa-P]** and **[Ru^{II}-hpa-P]** are 1.2 ± 0.1 and 0.97 ± 0.03 respectively, suggesting that **[Ru^{III}-hpa-P]** binds with CT-DNA more strongly than **[Ru^{II}-hpa-P]**. At lower concentrations, the Ru complex competitively inhibits the EB interaction whereas at higher concentrations, the complexes are noncompeting with the EB interaction. The above results suggest that the complexes

[Ru^{III}-hpa-P] and **[Ru^{II}-hpa-P]** efficiently bind with CT-DNA at lower concentrations only. This insight is in accordance with the electronic absorption spectral information.

Viscometric studies

The structural changes of DNA by binding with small molecules have been the authentic indication of the binding mode. Viscosity measurements are one of the traditional and still one of the most unambiguous methods to scrutinize DNA structural changes by the length changes of rod-like DNA. It has been proved that intercalative DNA binding with small molecules leads to an increase in viscosity, since the intercalative binding causes elongation of the DNA polymer by separation of the DNA base pairs.[33] The effect of the complexes on the viscosity of DNA is shown in Fig. 5. Complexes **[Ru^{II}-hpa-As]** and **[Ru^{III}-hpa-As]** actually have no effect on the viscosity of DNA, while complexes **[Ru^{III}-hpa-P]** and **[Ru^{II}-hpa-P]** decreased the relative viscosity of the DNA at a low mixing ratios ($R < 0.16$). The observed significant decreases in viscosity of DNA with the complexes **[Ru^{III}-hpa-P]** and **[Ru^{II}-hpa-P]** are similar to that of D-[Ru(phen)$_3$]$^{2+}$[34,35] which may be explained by a binding mode that produces bends or kinks in the DNA helix and thus reduces its effective length and, concomitantly, its viscosity. The viscosity results suggested that complexes **[Ru^{III}-hpa-P]** and **[Ru^{II}-hpa-P]** bind with DNA in a non-intercalative manner, possibly a groove binding mode.

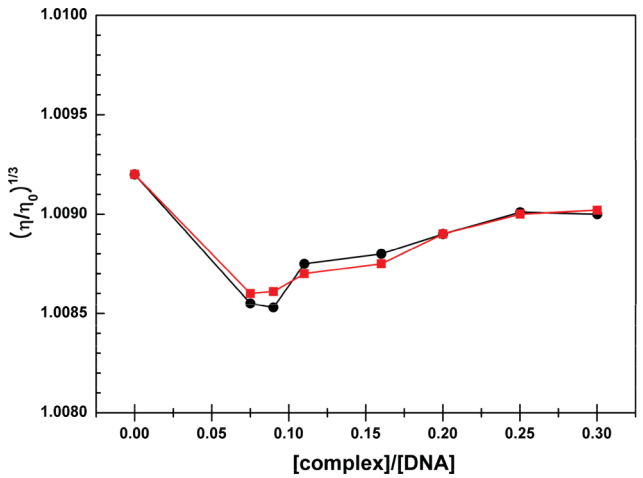

Fig. 5 Effect of increasing amounts of [Ru^{III}-hpa-P] (●) and [Ru^{II}-hpa-P] (■) on the relative viscosities of CT-DNA in 5 mM Tris-HCl buffer (pH 7.0).

Thermal denaturation experiments

Optical photophysical probes commonly provide basic, but not sufficient clues to ascertain the binding mode. The viscosity measurement was introduced as further support to elucidate the interaction between the metal complex and DNA. Additional strong evidence for binding of the ruthenium complexes to the double helix of DNA is a thermal denaturation experiment. The melting temperature (T_m) is defined as the temperature at which half of the DNA strands are in the double-helical state and half are in the "random-coil" state. A large change in the T_m of DNA is indicative of a strong interaction with DNA.[36] The melting profiles of denaturation of CT-DNA were measured by plotting the UV maximum absorption of DNA at 260 nm *versus* the temperature, in the absence and presence of ruthenium complexes at two different molar ratios R = [Ru]/[DNA] = 0, 0.2, and 0.07 (Fig. 6). The results revealed that the T_m of the free DNA duplex was 60.0 ± 0.1 °C, which was increased by 2 and 3 °C in the presence of complexes **[Ru^{II}-hpa-P]** and **[Ru^{III}-hpa-P]** respectively at low R ratios. This implies that they are non-intercalators because the relative absorbance is not so high compared to that of the pure DNA sample. At a high R ratio, no obvious change in the melting profile of DNA can be observed under the same measurement conditions. This scenario may indicate the interaction of the **[Ru^{II}-hpa-P]** and **[Ru^{III}-hpa-P]** with DNA is stronger at low mixing ratios ($R < 0.16$) than at higher ratios ($R > 0.16$), which is in consonance with the conclusions derived from the other studies given above. Under the same set of conditions, the addition of **[Ru^{II}-hpa-As]** and **[Ru^{III}-hpa-As]** to the double helical DNA had no appreciable effect on T_m of free DNA (data not shown). It is revealed that they did not interact substantially with DNA.

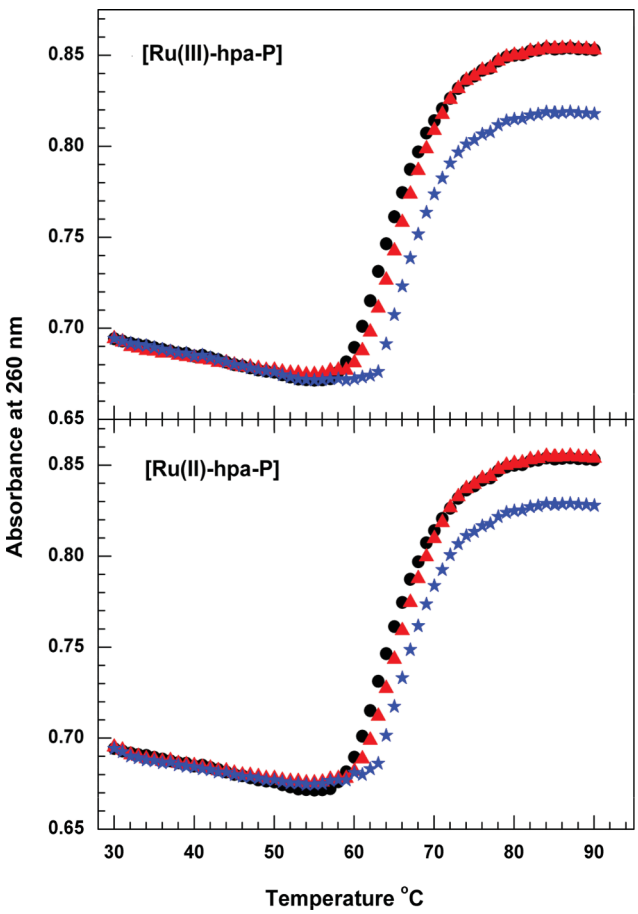

Fig. 6 Thermal denaturation plots of 100 μM CT-DNA alone (●) and in the presence of complexes at R = [Ru]/[DNA] = 0.2 (▲), 0.07 (★).

The planarity area (S) of a chelating ligand of the metal complex is surely an important factor because the larger the planarity area of the ligand, the greater the stacking interaction between the ligand and base pairs of DNA. From the above DNA binding results, it is obvious that the present ligand system lacks extended π-systems, ruling out the possibility of any intercalative

Table 5 Antioxidant activity of all the complexes, vitamin C and BHT against various radicals

Compounds	IC_{50}(μM)					
	DPPH$^{\bullet}$	OH$^{\bullet}$	NO$^{\bullet}$	$O_2^{-\bullet}$	H_2O_2	Metal chelating
[Ru^{II}-hpa-P]	55	42	53	39.6	55.5	59.6
[Ru^{II}-hpa-As]	62.7	53.6	60.9	57.2	66	73.7
[Ru^{III}-hpa-P]	19.6	11.5	18.2	13.8	23.9	32.7
[Ru^{III}-hpa-As]	26.5	17.1	25.2	24.4	31	38.8
Vitamin C	147.6	232.8	215.8	221.4	238.5	—
BHT	86.2	163.4	154.3	131.6	149.8	—

interaction, but has the potential to bind to DNA. The experimental results suggest that the complexes could bind DNA in two different modes. The binding behavior observed for the triphenylphosphine analog with double helical CT-DNA differs from triphenylarsine complexes. The **[Ru^{II}-hpa-P]** and **[Ru^{III}-hpa-P]** bind with double helical DNA in the groove binding mode whereas **[Ru^{II}-hpa-As]** and **[Ru^{III}-hpa-As]** bind by means of the electrostatic mode. This is related to the molecular structures of the complexes. Among the complexes examined, the triphenylarsine analog shows the lowest binding strength (electrostatic) to double-helical DNA. The difference in the binding modes between triphenylphosphine and triphenylarsine analogs may be due to the presence of bulky $AsPh_3$ groups *trans* to each other, which causes steric hindrance. It reveals that the effective binding strength of the chelating ligand (H_2hpa) towards the double helical DNA would be prevented by the steric clashes from the six phenyl rings of the *trans* $AsPh_3$ with the DNA surface. The steric clash involving co ligands and the DNA polymer would hinder the placement of the chelating rings in between the DNA helix. These steric clashes also appeared in the triphenylphosphine complexes but the potency is small when compared to the triphenylarsine analogs. These observations also indicate that the planarity of the chelating ligand in the complex has a significant effect on DNA binding affinity, which decreases in the order **[Ru^{III}-hpa-P]** > **[Ru^{II}-hpa-P]** > **[Ru^{II}-hpa-As]** ~ **[Ru^{III}-hpa-As].** The difference in DNA-binding properties of complexes is due to the different co-ligands and different oxidation states of the metal ion.

Antioxidative activity

Since the complexes exhibit reasonable DNA-binding affinity, it is considered worthwhile to study other potential aspects, such as antioxidant and antiradical activity. Hence, we carried out experiments to explore the free radical scavenging ability of the complexes, with the hope of developing potential antioxidants and therapeutic reagents for respiratory diseases, such as asthma, emphysema and asbestosis.[37] The IC_{50} values of all the complexes (Table 5 and Fig. S7, ESI†) obtained from different types of assay experiments strongly supports that they possess excellent antioxidant activities, which are better than those of standard antioxidants including the natural antioxidant vitamin C and the synthetic antioxidant BHT (butylated hydroxytoluene).

Free radicals can induce DNA damage in humans. The damage to DNA has been suggested to contribute to aging and various diseases including cancer and chronic inflammation.[38] The DPPH radical has been widely used to test the ability of compounds as free radical scavengers or hydrogen donors to evaluate the antioxidant activity. Hydrogen peroxide itself is not very reactive, but sometimes it is toxic to cells because it may give rise to hydroxyl radicals in the cells.[39] The free radical scavenger action is very important, especially in the case of the superoxide anion, since it prevents or attenuates the formation of peroxynitrite and hydroxyl radicals. The overproduction of peroxynitrite and hydroxyl radicals constitutes a very important feature regarding tissue damage mechanisms during pathological processes. Numerous biological reactions generate the superoxide radical, which is a highly toxic species, along with other reactive molecules that tend to react with cellular components such as membrane lipids and proteins, thereby disturbing their function and consequently cellular homeostasis.[40,41] Thus, the study of scavenging of this radical is important.[42] Nitric oxide or reactive nitrogen species, formed during their reaction with oxygen or with superoxide, such as NO_2, N_2O_4, N_3O_4, NO_3^- and NO_2^+ are very reactive. These species are responsible for altering the structural and functional behavior of many cellular components. Further, the scavenging activity may also help to arrest the chain of reactions initiated by excess generation of NO that is detrimental to human health. Among all free radicals, the hydroxyl radical is a major product arising from the high-energy ionization of water, the most important biological sources of which are the Haber–Weiss and Fenton reactions, involving the superoxide anion, hydrogen peroxide and transition metals.[43] This is the most aggressive oxidant known and therefore the most dangerous oxygen metabolite, which is capable of attacking any biological molecule and can be implicated in the tissue damage associated with inflammation, therefore elimination of this radical is one of the major aims of antioxidant administration.[44]

The two Ru^{II} complexes and the two Ru^{III} complexes with similar structures showed almost comparable antioxidant activities. In general, the Ru^{III} complexes showed better activity than the Ru^{II} complexes. This might be due to the d^5 low spin electronic configuration and the availability of an odd electron in Ru^{III} complexes, which increases the capacity to stabilize the unpaired electrons and thereby scavenge the free radicals. The electron deficient metal centers in Ru^{III} complexes might increase the acidity of the available ligand proton thereby increasing the antioxidant activity in terms of H^+ donors when compared to Ru^{II} complexes.

The hydroxyl radical scavenging power of the tested complexes was the greatest, and the metal chelating ability was the lowest. Being a potent scavenger of hydroxyl radicals, the complexes could capture superoxide anion radicals and hydrogen peroxide, as evident from the IC_{50} values. The metal chelating ability of the tested complexes is poor owing to the lack of active groups for chelation, and might be the weak interaction between the

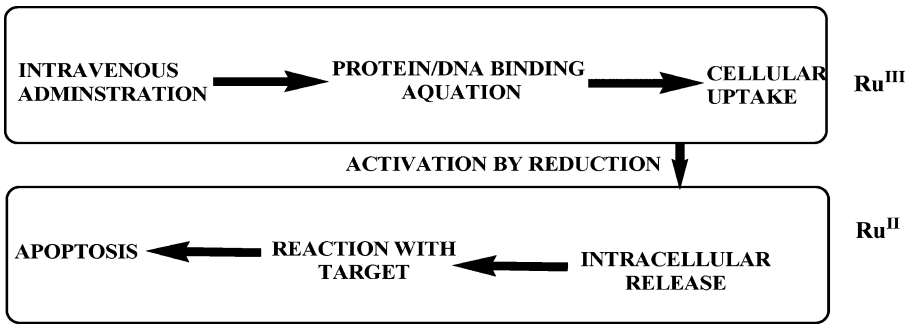

Scheme 2 Proposed mode of action of ruthenium anticancer agents.

complexes and Fe^{2+}. Although the radical scavenging mechanism of the complexes under study remains unclear, the experimental results are helpful in designing more effective antioxidant agents against free radicals.

Cytotoxic activity evaluation by MTT assay

Kinetic lability/inertness toward ligand substitution is a major determinant that controls the covalent interactions of a metal complex with biological target molecules. Ru^{III} complexes probably act as prodrugs that are relatively inert toward ligand substitution and therefore their anticancer activity depends on the ease of reduction to more labile plus kinetically more reactive Ru^{II} complexes. The resulting Ru^{II} species are generally less inert, have a high propensity for ligand exchange reactions and may therefore interact with target molecules more rapidly.[45–47]

We intended to verify this bioreductive activation mechanism (Scheme 2) under *in vitro* conditions, and hence, cytotoxicity studies were carried out. Moreover, as the balance between the therapeutic potential and toxic side effects of a compound is very important when evaluating its usefulness as a pharmacological drug, experiments were designed to investigate the *in vitro* cytotoxicity of synthesized ruthenium complexes and a benchmark compound cisplatin, against three human cancer lines including HeLa, HepG2, HEp-2 and the normal cell line NIH 3T3. Cytotoxicity was determined by means of a colorimetric microculture MTT assay, which measures mitochondrial dehydrogenase activity as an indication of cell viability. The IC_{50} values of four ruthenium complexes and cisplatin for selected cell lines which show interesting results are presented in Table 6. It is evident from the graphs (Fig. S8–S11, ESI†) that the number of cells decreased with an increase in the concentration of the complexes. With regard to the hypothesized bioreductive activation mechanism, the Ru^{II} complexes showed higher potential antineoplastic activity than did the Ru^{III} complexes, as evidenced by the lower IC_{50} values. The low O_2 content and lower pH in tumor cells should favor Ru^{II}, which is generally supposed to coordinate more readily with biomolecules than Ru^{III},[48] and thus provide for selective toxicity. Some promising cytotoxic effects were observed for Ru^{II} complexes toward the HepG2 and HeLa cell lines as reported in Table 6, even though they were slightly lower than cisplatin. These results are much better than those previously reported for other Ru^{II} complexes.[49] With HepG2, the **[Ru^{II}-hpa-P]** appears to satisfy the conditions for carrying out the "cisplatin magic" (differential reactivity in inter and intracellular media and its capacity to bind DNA bases) in inhibiting the growth of the cancer cell. Despite this potency, **[Ru^{II}-hpa-P]** and **[Ru^{II}-hpa-As]** were much less toxic toward normal cells, with IC_{50} values at 248 and 187 μM respectively, which are significantly higher than those of cisplatin (177 μM). These results suggest that they possess great selectivity between cancer and normal cells and display application potential in cancer chemoprevention and chemotherapy. Cytotoxic effects of **[Ru^{III}-hpa-P]** and **[Ru^{III}-hpa-As]** are only low to moderate on the tested cell lines and the complex **[Ru^{III}-hpa-As]** did not show any significant activity even up to 128–353 μM concentration on HeLa and HepG2 cell lines. This might be due to the need to reduce them to Ru^{II} before they can exert their action.

Table 6 IC_{50} (μM) ruthenium complexes and cisplatin against various cancer cell lines

	IC_{50}(μM)[a]			
Complexes	HeLa	HepG2	HEp-2	NIH 3T3
[Ru^{II}-hpa-P]	27	22	23	248
[Ru^{II}-hpa-As]	31	32	35	187
[Ru^{III}-hpa-P]	75	73	50	124
[Ru^{III}-hpa-As]	128	353	63	109
Cisplatin	16	20	09	177

[a] fifty percent inhibitory concentration after exposure for 48 h in the MTT assay

Conclusion

A series of Ru^{II} and Ru^{III} complexes containing 4-hydroxypyridine-2,6-dicarboxylic acid and PPh_3/$AsPh_3$ have been prepared. The structures were established by X-Ray crystallography and spectroscopic methods. Furthermore, they were characterized with regard to drug-like properties such as DNA interactions, radical scavenging ability and tumor-inhibiting potential in a cancer cell line panel. The influence of nature and size of the co-ligands in the complexes on binding with DNA was demonstrated. The fine points obtained from various antioxidant assays showed that the Ru^{III} complexes exhibited excellent radical scavenging activities against hydroxyl radical, superoxide anion radical, nitric oxide radical, DPPH radical and hydrogen peroxide. Moreover, the cytotoxic studies showed that Ru^{II} complexes displayed less toxicity on normal cells and significant cytotoxic activity against HepG2 and HeLa cell lines, different from that of Ru^{III} complexes. The findings described should be considered in the future design of ruthenium pharmaceuticals to successfully predict the role of the

ligand and the Ru^{III}/Ru^{II} redox properties on anticancer activities, although the generality of some of the above conclusions has still to be tested with a wider variety of ruthenium complexes, which is in progress in our laboratory.

Acknowledgements

This research was supported by Department of Science and Technology, New Delhi, India [Grant No. SR/SI/IC-43/2007], and Nuclear R&D Programs through the National Research Foundation of Korea (NRF) funded by Ministry of Education, Science and Technology [Grant No. 2010-0018365, 2011-0002262].

References

1 Metal-based drugs: (*a*) C. Orvig and M. J. Abrams, *Chem. Rev.*, 1999, **99**, 2201–2842; (*b*) Z. Guo and P. J. Sadler, *Angew. Chem., Int. Ed.*, 1999, **38**, 1512–1531; (*c*) N. Farrell, *Coord. Chem. Rev.*, 2002, **232**, 1–230; (*d*) D. Schlawe, A. Majdalani, J. Velcicky, E. Heßler, T. Wieder, A. Prokop and H. G. Schmalz, *Angew. Chem., Int. Ed.*, 2004, **43**, 1731–1734; (*e*) P. J. Dyson and G. Sava, *Dalton Trans.*, 2006, 1929–1933; (*f*) U. Schatzschneider and N. Metzler-Nolte, *Angew. Chem., Int. Ed.*, 2006, **45**, 1504–1507; (*g*) W. H. Ang and P. J. Dyson, *Eur. J. Inorg. Chem.*, 2006, 4003–4018.
2 Z. Guo and P. J. Sadler, *Angew. Chem., Int. Ed.*, 1999, **38**, 1512–1531.
3 Z. Guo and P. J. Sadler, *Adv. Inorg. Chem.*, 2000, **49**, 183–306.
4 V. B. Arion, E. Reisner, M. Fremuth, M. A. Jakupec, B. K. Keppler, V. Yu. Kukushkin and A. J. L. Pombeiro, *Inorg. Chem.*, 2003, **42**, 6024–6031.
5 P. J. Sadler, *Adv. Inorg. Chem.*, 1991, **36**, 1–48.
6 M. J. Cleare and J. D. Hoeschele, *Bioinorg. Chem.*, 1973, **2**, 187–210.
7 R. D. Murdoch and J. Pepys, *Int. Arch. Allergy Immunol.*, 1985, **77**(4), 456–458.
8 H. M. Pineto and J. H. Schornagel (ed.), *Platinum and Other Metal Coordination Compounds in Cancer Chemotherapy*, Plenum, New York, 1996.
9 P. C. Bruijnincx and P. J. Sadler, *Curr. Opin. Chem. Biol.*, 2008, **12**, 197–206.
10 C. M. Che and J. Sh. Huang, *Coord. Chem. Rev.*, 2002, **231**, 151–164.
11 G. Sava, I. Capozzi, A. Bergamo, R. Gagliardi, M. Cocchietto, L. Masiero, M. Onisto, E. Alessio, G. Mestroni and S. Garbisa, *Int. J. Cancer*, 1996, **68**, 60–66.
12 M. Galanski, V. B. Arion, M. A. Jakupec and B. K. Keppler, *Curr. Pharm. Des.*, 2003, **9**, 2078–2089.
13 Y. K. Yan, M. Melchart, A. Habtemariam and P. J. Sadler, *Chem. Commun.*, 2005, 4764–4776.
14 W. H. Ang and P. J. Dyson, *Eur. J. Inorg. Chem.*, 2006, **20**, 4003–4018.
15 (*a*) A. Pasini and F. Zunino, *Angew. Chem., Int. Ed. Engl.*, 1987, **26**, 615–624; (*b*) R. C. Harrison and C. A. Mcauliffe, *Inorg. Chim. Acta*, 1980, **46**, L15–L16.
16 G. J. Bridger, R. T. Skerlj, S. Padmanabhan, S. A. Martellucci, G. W. Henson, S. Struyf, M. Witvrouw, D. Schols and E. D. Clercq, *J. Med. Chem.*, 1999, **42**, 3971–3981.
17 K. Naresh Kumar and R. Ramesh, *Polyhedron*, 2005, **24**, 1885–1892.
18 Y. P. Tian, M. L. Zhang, Z. J. Hu, H. M. Hu, J. Y. Wu, X. J. Zhang, X. T. Tao, M. H. Jiang, H. P. Chen, S. Chantrapromma and H. K. Fun, *Transition Met. Chem.*, 2005, **30**, 778–785.
19 A. W. Wallace, W. R. Murphy Jr and J. D. Peterson, *Inorg. Chim. Acta*, 1989, **166**, 47–54.
20 F. Basuli, S. M. Peng and S. Bhattacharya, *Inorg. Chem.*, 2001, **40**, 1126–1133.
21 R. S. Srivastava and F. R. Fronczek, *Inorg. Chim. Acta*, 2001, **322**, 32–36.
22 A. Hijazi, J. P. Djukic, M. Pfeffer, L. Ricard, N. K. Gruber, J. Raya, P. Bertani and A. De. Cian, *Inorg. Chem. Commun.*, 2006, **45**, 4589–4591.
23 N. Chitrapriya, V. Mahalingam, M. Zeller and K. Natarajan, *Polyhedron*, 2008, **27**, 1573–1580.
24 P. Sengupta, R. Dinda, S. Ghosh and W. S. Sheldrick, *Polyhedron*, 2001, **20**, 3349–3354.
25 P. Sengupta, S. Ghosh and T. C. W. Mak, *Polyhedron*, 2001, **20**, 975–980.
26 S. A. Serron, C. M. Haar, S. P. Nolan and L. Brammer, *Organometallics*, 1997, **16**, 5120–5123.
27 D. Ooyama and M. Sato, *Anal. Sci.*, 2003, **19**, 39–42.
28 D. Sukanya, R. Prabhakaran and K. Natarajan, *Polyhedron*, 2006, **25**, 2223–2228.
29 S. M. Couchman, J. M. D. Vera, J. C. Jeffery, C. A. Mckee, S. Nevitt, M. Pohlman, C. M. White and M. D. Ward, *Polyhedron*, 1998, **17**, 3541–3550.
30 M. Cory, D. D. Mckee, J. Kagan, D. W. Henry and J. A. Miller, *J. Am. Chem. Soc.*, 1985, **107**, 2528–2536.
31 G. Psomas, *J. Inorg. Biochem.*, 2008, **102**, 1798–1811.
32 P. J. Cox, G. Psomas and C. A. Bolos, *Bioorg. Med. Chem.*, 2009, **17**, 6054–6062.
33 J. G. Liu, Q. L. Zhang, X. F. Shi and L. N. Ji, *Inorg. Chem.*, 2001, **40**(19), 5045–5050.
34 S. Satyanarayana, J. C. Dabrowiak and J. B. Chaires, *Biochemistry*, 1992, **31**, 9319–9324.
35 S. Satyanarayana, J. C. Dabrowiak and J. B. Chaires, *Biochemistry*, 1993, **32**, 2573–2584.
36 Y. An, S. D. Liu, S. Y. Deng, L. N. Ji and Z. W. Mao, *J. Inorg. Biochem.*, 2006, **100**, 1586–1593.
37 A. Bast, G. R. M. M. Haenen and C. J. A. Doelman, *Am. J. Med.*, 1991, **91**, 2–13.
38 K. Tsai, T. G. Hsu, K. M. Hsu, H. Cheng, T. Y. Liu, C. F. Hsu and C. W. Kong, *Free Radical Biol. Med.*, 2001, **31**, 1465–1472.
39 B. Halliwell, *Am. J. Med.*, 1991, **91**, 14–22.
40 D. A. Wink and J. B. Mitchell, *Free Radical Biol. Med.*, 1998, **259**(4-#x2013;5), 434–456.
41 J. P. Kehrer, *Crit. Rev. Toxicol.*, 1993, **23**, 21–48.
42 S. R. Kannat, R. Chander and A. Sharma, *Food Chem.*, 2007, **600**, 451–458.
43 J. M. C. Gutteridge, *Chem.-Biol. Interact.*, 1994, **91**, 133–140.
44 N. Udilova, A. V. Kozlov, W. Bieberschulte, K. Frei, K. Ehrenberger and H. Nohl, *Biochem. Pharmacol.*, 2003, **65**, 59–65.
45 M. J. Clarke, S. Bitler, D. Rennert, M. Buchbinder and A. D. Kelman, *J. Inorg. Biochem.*, 1980, **12**, 79–87.
46 M. J. Clarke, *Prog. Clin. Biochem. Med.*, 1989, **10**, 25–39.
47 M. J. Clarke, *Coord. Chem. Rev.*, 2003, **236**, 209–233.
48 A. D. Kelman, M. J. Clarke, S. D. Edmonds and H. J. Peresie, *J. Clin. Hematol. Oncol.*, 1977, **7**, 274–288; M. J. Clarke, In *Metal Complexes in Cancer Chemotherapy*, B. K. Keppler, Ed., VCH, Weinheim, 1993, 129-157.
49 (*a*) F. Gao, X. Chen, J. Q. Wang, Y. Chen, H. Chao and L. N. Ji, *Inorg. Chem.*, 2009, **48**(13), 5599–5601; (*b*) D. L. Ma, C. M. Che, F. M. Siu, M. Yang and K. Y. Wong, *Inorg. Chem.*, 2007, **46**(3), 740–749.
50 N. Ahmed, J. J. Lewison, S. D. Robinson and M. F. Uttley, *Inorg. Synth.*, 1974, **15**, 48.
51 R. A. S. Pelgado, W. Y. Lee, S. R. Choi, Y. Cho and M. J. Jun, *Transition Met. Chem.*, 1991, **16**, 241–244.
52 J. Chatt, G. J. Leigh, D. M. P. Mingos and R. J. Parke, *J. Chem. Soc. A*, 1968, 2636–2641.
53 R. K. Poddar, I. P. Khullar and U. Agarwala, *Inorg. Nucl. Chem. Lett.*, 1974, **10**, 221–227.
54 A. I. Vogel, *Textbook of Practical Organic Chemistry*, 5th ed., Longman, London, 1989.
55 A. L. Spek, *Acta Crystallogr., Sect. D: Biol. Crystallogr.*, 2009, **65**, 148.
56 M. C. Altomare, M. Burla, G. Camalli, C. Cascarano, A. Giacovazzo, A. G. G. Guagliardi, G. Moliterni and R. Polidori, *J. Appl. Crystallogr.*, 1999, **32**, 115–122.
57 G. M. Sheldrick, *SHELXL-97, Program for Structure Refinement*, University of Göttingen, Göttingen, Germany, 1997.
58 L. J. Farrugia, *J. Appl. Crystallogr.*, 1997, **30**, 565–566.
59 M. S. Blois, *Nature*, 1958, **29**, 1199–1200.
60 T. Nash, *Biochem. J.*, 1953, **55**, 416–421.
61 L. C. Green, D. A. Wagner, J. Glogowski, P. L. Skipper, J. S. Wishnok and S. R. Tannenbaum, *Anal. Biochem.*, 1982, **126**, 131–138.
62 R. J. Ruch, S. J. Cheng and J. E. Klaunig, *Carcinogenesis*, 1989, **10**, 1003–1008.
63 C. Beauchamp and I. Fridovich, *Anal. Biochem.*, 1971, **44**, 276–287.
64 T. C. P. Dinis, V. M. C. Madeira and L. M. Almeida, *Arch. Biochem. Biophys.*, 1994, **315**, 161–169.
65 M. Blagosklonny and W. S. EI-diery, *Int. J. Cancer*, 1996, **67**(3), 386–392.